RESEARCH ARTICLE | JUNE 23 2025

An ultra-compact deterministic source of maximally entangled photon pairs

M. Langer ; P. Ruchka ; A. Rahimi ; S. Jakovljevic ; Y. G. Zena ; S. A. Dhurjati ; A. Danilov; M. Pal; R. Bassoli ; F. H. P. Fitzek ; O. G. Schmidt ; H. Giessen ; C. Hopfmann

APL Photonics 10, 066117 (2025)
https://doi.org/10.1063/5.0271023

APL Photonics ARTICLE pubs.aip.org/aip/app

An ultra-compact deterministic source of maximally entangled photon pairs

Cite as: APL Photon. 10, 066117 (2025); doi: 10.1063/5.0271023
Submitted: 14 March 2025 • Accepted: 7 June 2025 •
Published Online: 23 June 2025

M. Langer,[1] P. Ruchka,[2] A. Rahimi,[1] S. Jakovljevic,[2] Y. G. Zena,[1] S. A. Dhurjati,[1] A. Danilov,[1] M. Pal,[1] R. Bassoli,[3] F. H. P. Fitzek,[4] O. G. Schmidt,[5] H. Giessen,[2,a)] and C. Hopfmann[1,3,b)]

AFFILIATIONS

[1] Institute for Emerging Electronic Technologies, IFW Dresden, Helmholtzstraße 20, 01069 Dresden, Germany
[2] 4th Physics Institute and Research Center SCoPE, University of Stuttgart, 70569 Stuttgart, Germany
[3] Quantum Communication Networks research group, Deutsche Telekom Chair of Communication Networks, Technische Universität Dresden, Dresden, Germany
[4] Deutsche Telekom Chair of Communication Networks, Technische Universität Dresden, Dresden, Germany
[5] Research Center for Materials, Architectures and Integration of Nanomembranes (MAIN), Chemnitz University of Technology, Chemnitz, Germany

[a)] **Electronic mail:** giessen@pi4.uni-stuttgart.de
[b)] **Author to whom correspondence should be addressed:** caspar_arndt.hopfmann@tu-dresden.de

ABSTRACT

We demonstrate an ultra-compact source of on-demand, maximally entangled photon pairs using single GaAs quantum dots embedded in monolithic microlenses coupled to a lensed single-mode fiber. A 3D-printed micro-objective with a numerical aperture of 0.6 enables efficient fiber coupling and near-diffraction-limited performance with 604(16) nm resolution directly in the cryogenic environment at 3.8 K. The system achieves high single-photon emission rates [392(20) kHz] and purities [99.2(5)%] using two-photon resonant excitation. Leveraging the exciton–biexciton cascade, it produces near-maximally entangled photon pairs with peak entanglement negativities of $2n = 0.96 \pm 0.02$. The presented quantum light source combines state-of-the-art performance and long-term stability with a dramatically reduced system footprint, making it well-suited for seamless industrial integration.

I. INTRODUCTION

In the quest for realizing quantum communication networks,[1,2] significant progress has been made in the past decade by realizing high-performing quantum light sources.[3–13] In order to realize multipartite quantum networks, entangled photon sources are a key component.[14,15] While sources based on parametric down-conversion have been very successful[16,17]—partly due to their relative ease of implementation using non-linear optics—the performance of these sources remains fundamentally limited to their classical Poissonian statistics.[18] Specifically, on-demand entangled photon pair sources with high efficiencies, entanglement fidelities, and indistinguishabilities are crucial in order to enable Bell-state interferences necessary to build multipartite quantum information exchange networks and quantum repeater systems[1,14] enabling applications such as distributed quantum computing[19] and physically secure communication.[20] Quantum light sources such as semiconductor quantum dots (QDs), color centers in diamond, and trapped atoms or ions can potentially realize this kind of quantum light sources, as they do not suffer from the same limitations due to their Fock state-like quantum photon number distributions.[14,21] In recent years, semiconductor QDs, and especially droplet etched GaAs QDs, have been firmly established as efficient solid-state sources of highly entangled photon pairs[4,22,23] utilizing the resonantly driven exciton–biexciton cascade.[6,7,13,24,25] In order to attain highly coherent and efficient quantum light sources, a high degree of control of the interactions between the quantum system and its environment is required—in solid-state systems this is commonly achieved by cooling to cryogenic temperatures, typically below 10 K. Due to this premise, it is highly challenging to miniaturize the realized sophisticated sources and make them suitable for industrial environments—such as server rooms—which is a prerequisite to realize practical implementations of quantum networks on a large scale. Furthermore, as today's communication infrastructure relies heavily on data exchange via optical fibers and unstabilized free-space optical systems are unsuitable for industrial environments—such as 19*in*-rack systems—compact, mobile, and *in situ* fiber-coupled quantum light sources are very desirable. While deterministically fabricated, compact, and fiber-coupled single photon sources based on InGaAs QDs have been explored,[26–28] their performance is orders of magnitude lower compared to cavity-based light extraction[5,7,10] and free-space collection approaches.[3,6] To address this challenge, a viable design of an efficient, ultra-compact, and fiber-coupled entangled photon pair source based on the droplet-etched GaAs QD platform is presented in this work. By realizing such a device, we expect our work to contribute toward scalable out-of-lab realizations of future entanglement-based quantum communication networks.

II. SYSTEM DESIGN

In order to realize the desired fiber-coupled, ultra-compact, efficient, and on-demand entangled photon pair sources based on semiconductor quantum dots (QDs), it is necessary to couple the emission of the QDs operated at cryogenic temperatures efficiently to single mode fibers. This entails extracting the emitted light from high refractive index matrix material semiconductors, such as GaAs, exhibiting refractive indices of about 3.5.[29] Due to the small angle of total internal reflection at the surface of these materials, engineering of the QD photonic environment is required to achieve efficient photon extraction.[30] Strategies for high-performance extraction from semiconductors have been realized using various methods, such as open fiber, circular Bragg and photonic crystal cavities,[7,10,12] and monolithic micro- and semiconductor solid immersion lenses.[6,31] In addition, the extracted light from the semiconductor quantum light sources needs to be efficiently inserted into a single mode fiber inside the cryogenic environment. This is necessary in order to keep the footprint of the system small and achieve compatibility with industrial environments—such as server rooms—because in these environments the employment of free-space optics needs to be avoided as vibration and temperature stability are limited.

It has been shown many times that GaAs QDs in $Al_{0.15}Ga_{0.85}As$ matrix material are excellent sources of on-demand and maximally entangled photon pairs using their inherent exciton (X)–biexciton (XX) cascade using a two-photon excitation scheme.[6,13,24,32] In order to attain efficient entangled photon pair sources from these QDs, both X and XX emissions need to be efficiently coupled. Since the typical energy splitting of these emission lines is about 3.6 meV,[33] microcavities with high Q-factors, i.e., small bandwidths, cannot be used for efficient light extraction of entangled photon pairs. For this reason, open-fiber cavities are not suitable for QD-based entangled photon sources, even though these systems have demonstrated very high extraction efficiencies of single photons from QDs into single mode fibers of up to 57%.[10] In previous work, we have shown that QD-nanomembranes attached to *GaP* solid immersion lenses can be used to realize efficient sources of entangled photon pairs.[6] However, due to their macroscopic nature, they are fundamentally unsuited for direct fiber coupling inside a compact cryostat, as a macroscopic objective with high numerical aperture (NA) would be required to insert the entangled photon pairs into a single mode fiber. The latter can only be achieved in large cryostats unsuitable for operation in industry standard rack-systems. This leaves microscopic devices such as monolithic microlenses and circular Bragg cavities to achieve efficient extraction of entangled photon pairs. In this work, we chose the approach of monolithic microlenses, as these are inherently broadband and polarization insensitive microscale devices. To achieve the same with circular Bragg cavities of moderate Q-factor would require very precise positioning of the QD with respect to the microcavity.[7,8]

To provide efficient light extraction of the QDs from the $Al_{0.15}Ga_{0.85}As$ matrix material, monolithic microlenses are used. A comprehensive and detailed analysis of the fabrication process, its optimization, and performance statistics is found in our recent publication, Ref. 34. Further details can also be found in the supplementary material, Sec. I A. The shape of the monolithic microlenses and the sample layout used in this work are discussed in Sec. III and the supplementary material, Fig. S1, respectively. It is worth noting that in the present work, the alignment between $Al_{0.15}Ga_{0.85}As$ microlenses and QDs is not controlled. In order to achieve high extraction efficiencies, one has to postselect lenses with centrally embedded QDs. Based on the QD density of about $0.2/\mu m^2$ and simulations, it can be estimated that the chance of finding a lens with a QD above 80% of the theoretical maximum extraction efficiency is about 2%. The identification of efficient QD entangled photon pair sources therefore requires characterization of many lenses using, for example, the hyperspectral imaging technique described in Sec. III.

In order to tackle the challenge of efficient insertion of light emitted by single QDs into a single-mode fiber in a compact format at low temperatures, it is necessary to provide a high-NA optical system with a small footprint. It has been previously demonstrated that 3D-printed micro-objectives can be fabricated by two-photon polymerization technique directly on the end of standard single mode fibers.[35] Using this technique, it was possible to achieve rather complex designs with lensed fibers and 3D-printed lenses on QDs. This approach has been used to couple the emission of single InGaAs QDs using 3D-printed objectives featuring NAs of circa 0.13 by gluing the components together.[26,28,36] While these achievements are considerable, the published single photon rate using pulsed excitation was limited to values below 100 kHz. The reason for this is that once glued, there is no possibility to adjust the mechanical alignment in any way;[37] any temperature induced shift cannot therefore be compensated for.[38] Furthermore, in order to collect more light emitted by a QD, coupling optics with higher NA is needed. So far, achieving high-NA 3D-printed micro-objectives requires complex designs with several lenses.[39] These devices exhibit a significant drawback for coupling applications at cryogenic temperatures: such bulk 3D-printed structures are fragile and susceptible to temperature changes, especially because elements with different thermal expansion coefficients are combined. Recently, it has been shown that using no-core fibers is a promising approach to achieve high-NA 3D-printed micro-objectives on fibers using a single 3D-printed lens.[40] Therefore, the design of the 3D-printed micro-objective optimized for 780 nm employed in this work uses the latter approach of only one aspheric lens in combination with a spliced no-core

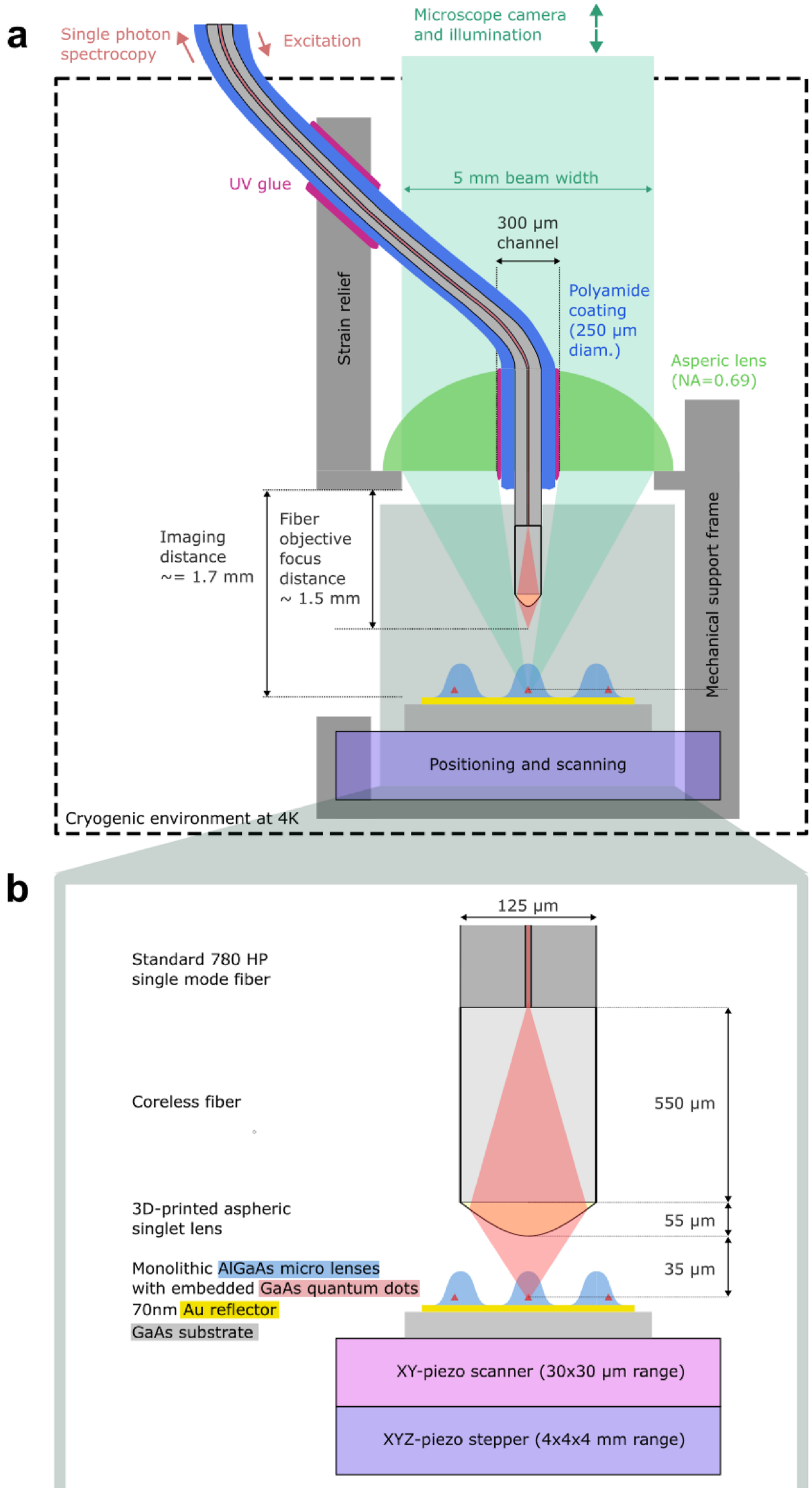

FIG. 1. Schematic illustration of the design of the ultra-compact fiber-coupled entangled photon pair source. The entangled photons emitted by the GaAs quantum dots embedded in monolithic microlenses are collected directly in the cryostat into a single mode fiber using a 3D-printed micro-objective. (a) Overall system optical and mechanical design overview, including supplementary free-space microscopy for rough positioning of the fiber micro-objective as well as fiber strain relief and mechanical support. (b) Detailed illustration of the collection optics and spatial positioning of entangled photon pairs from a single GaAs quantum dot embedded in monolithic microlenses.

fiber of about 500 μm length (see Fig. 1). By replacing the support structure (i.e., the 3D-printed expansion cylinder) with the piece of no-core glass fiber, the micro-objective becomes significantly more robust against mechanical shock and temperature drifts. Furthermore, we iteratively optimize the shape of the aspheric lens to compensate for the shape deviations caused by two-photon polymerization 3D-printing. The combination of beam expansion in the no-core fiber piece with the highly aspheric optimized lens allows us to achieve NAs of up to 0.6. Finally, instead of gluing the components together, fiber and sample mounts are engineered with the flexibility to be aligned using mechanical piezo stepper (range of 4 mm) and scanner (range of 30 μm) stages inside the cryostat. This provides the required flexibility to compensate for temperature drifts and enables long-term system stability. The overall experimental system design is further detailed in the supplementary material, Sec. I.

Figure 1(a) depicts the lensed fiber of type 780HP[41] that is glued into a 300 μm hole drilled into a standard 0.69 NA aspheric lens. The fiber with the attached 3D-printed micro-objective is glued into the aspheric lens so that the tip of the fiber-objective has a distance of ~1.5 mm, while the working distance of the lens is 1.7 mm. The purpose of this arrangement is to be able to image the surface of the sample to find specific microstructures. Once found, the sample can be moved up by circa 200 μm in order to collect the signal of the selected microstructure directly by the fiber micro-objective. When operated as an entangled photon pair source, the coarse imaging arrangement is inactive; it therefore does not affect the performance of the entangled photon pair source operation. In order to avoid any mechanical changes to the lensed fiber, it is secured in the cryostat using a strain relief and UV-glue.

III. RESULTS AND DISCUSSION

To determine the practical usability of the optical system designed in Sec. II and the scanning micro-objective lensed fiber system in particular, the optical performance characteristics need to be evaluated. To this end, the system is tested using hyperspectral imaging of a monolithic $Al_{0.15}Ga_{0.85}As$ microlens array. By comparing the nominal sample layout (cf. supplementary material, Fig. S1) with high resolution scanning electron microscopy (SEM) beam images [cf. Fig. 2(a)] and with the wavelength- and position-resolved signal of the sample shown in Figs. 2(b) and 2(c), respectively, the spatial displacement driven by the open-loop piezo scanners can be calibrated accurately. The experimental setup used for recording this hyperspectral imaging signal is detailed in the supplementary material, Sec. I E. The laser reflection signal is maximal in-between the monolithic $Al_{0.15}Ga_{0.85}As$ microlenses, while the luminescence signal of the microlenses (i.e., the band between 730 and 750 nm) behaves complementarily. When investigating the QD emission band of 770–790 nm, it is found that only a fraction of the monolithic microlenses feature centrally embedded QDs. On close inspection, one can find that some lenses feature weak signals from non-centrally embedded QDs.

In order to evaluate the limits of the optical and position-resolved performance of the scanning 3D-printed micro-objective at low temperatures, a detailed scan of a single microlens with

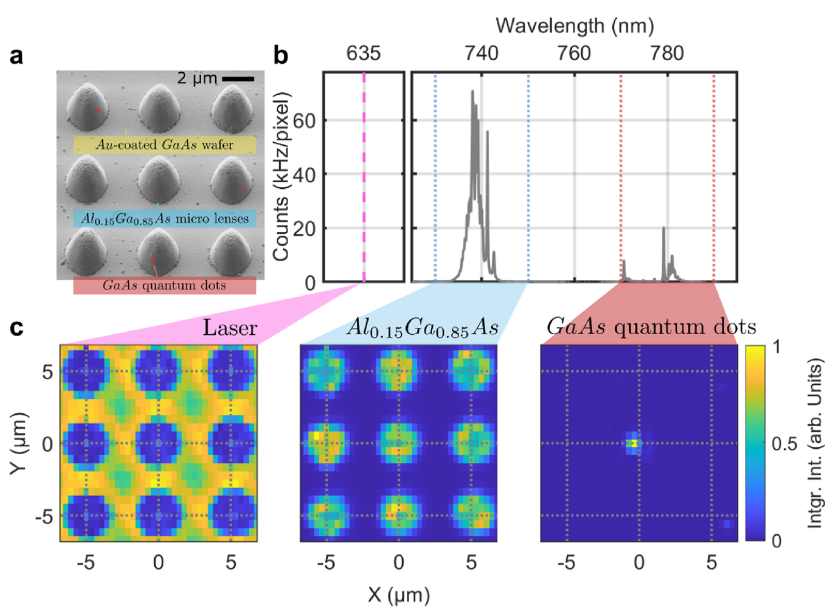

FIG. 2. (a) Scanning electron beam microscopy image recorded at an angle of 45° of an array of $Al_{0.15}Ga_{0.85}As$ monolithic microlenses on a gold-coated GaAs wafer. (b) Exemplary photoluminescence spectrum using 635 nm laser excitation collected through the single mode fiber using the 3D-printed micro-objective, cf. Fig. 1(b). The wavelength bands at 635, 730–750, and 770–790 nm of the excitation laser and the luminescence of the $Al_{0.15}Ga_{0.85}As$ matrix material and of the GaAs quantum dots are indicated in purple, light blue, and light red, respectively. (c) Representation of the three distinct hyperspectral micrographs obtained by recording the different photoluminescence and reflection bands at wavelengths (λ) of the reflected laser, the $Al_{0.15}Ga_{0.85}As$ monolithic microlenses, and GaAs quantum dots, respectively, as a function of spatial position using the XY-piezo scanner, cf. Fig. 1(b). All micrographs are obtained simultaneously using the experimental apparatus detailed in the supplementary material, Sec. I.

embedded quantum dots is performed. This hyperspectral image, together with comparable micrographs from atomic force (AFM) and SEM microscopy, is shown in Fig. 3. Raw AFM and SEM micrographs are shown in Fig. 3(a), while the extracted radial profile of a microlens is depicted in Fig. 3(b). One can deduce that the lens shape is in-between that of an ideal hemispherical and a Gaussian shaped lens. The performance of the microlenses is best when they are close to a hemispherical shape, because this allows for the smallest possible angle of the emitted light of a centrally embedded QD at the semiconductor–air interface. Beam shaping of the emitted light into reduced emission angles (i.e., with <1 NA) should be regarded as a secondary goal of the monolithic microlens design. The effects of the shape of QD monolithic microlens devices through combined simulation and experimental verification are discussed in great detail in our recent publication, Ref. 34. Based on these findings, which are attained by using microlens devices equivalent to the ones in this work, theoretical fiber-coupled efficiencies of up to 24% and 21% for ideal hemispherical and fabricated lens shapes, respectively, can be achieved. These investigations show, furthermore, that deployment of anti-reflection coatings on the monolithic microlenses could improve these efficiencies to values of up to 37% and 39%, respectively. Further enhancements are possible by increasing the NA of the fiber collection optics. The hyperspectral images shown in Fig. 3(c) corroborate the observations with the SEM and AFM microscopes very well. The determined lens diameter of 3.0(3) μm in the reflection and $Al_{0.15}Ga_{0.85}As$ bands demonstrates this nicely. If a QD is embedded centrally, as in this case, its spectral emission obtained in above-band excitation is enhanced by a factor of about 100 as compared to a quantum dot in an unprocessed $Al_{0.15}Ga_{0.85}As$ matrix material. Note that both brightness and position of the QDs inside the lens can be imaged and characterized using the scanning microlensed fiber setup. The spectral resolution of the 3D-printed microlensed fiber at cryogenic temperatures is investigated using a QD in an unprocessed part of the QD-nanomembrane of the same sample (cf. supplementary material, Fig. S1). The GaAs QDs in $Al_{0.15}Ga_{0.85}As$ typically feature sizes of 40 nm and are, therefore, significantly smaller than the wavelength of light inside the material of ~240 nm. Therefore, the width of the resulting position dependent QD luminescence curve is in good approximation that of the point spread function of the 3D-printed micro-objective. Using this method, the FWHM resolution limit of the micro-objective is determined to be 604(16) nm (cf. supplementary material, Fig. S5). This value is within the expected theoretical diffraction limit of $d_{\mathrm{FWHM}} = 0.51\lambda/\mathrm{NA} = 663$ nm, assuming the nominal numerical aperture of 0.6 and wavelength of 780 nm. Note that the actual NA value can vary slightly for the fabricated micro-objective employed in this work, thereby explaining the mismatch of the observed to the theoretical limit. Nevertheless, it is clear that the 3D-printed micro-objective is operating close to or even at the far field diffraction limit, thereby demonstrating the validity of the chosen design approach.

In addition to characterizing the basic optical performance parameters discussed above, a major goal of this work is to determine the suitability of the combination of monolithic QD-microlenses with 3D-printed fiber collection optics as ultra-compact entangled photon pair sources. To this end, the bright QD observed in Fig. 3 is subjected to pulsed resonant two-photon excitation (TPE). This excitation scheme enables resonant driving of the *XX* via absorption of two photons with an energy in-between the *X* and *XX* transitions [see Figs. 4(a) and 4(b)]. Due to the coherent nature of this excitation scheme, Rabi oscillations are observed as a function of the pulse power. This can be seen clearly in Fig. 4(c),

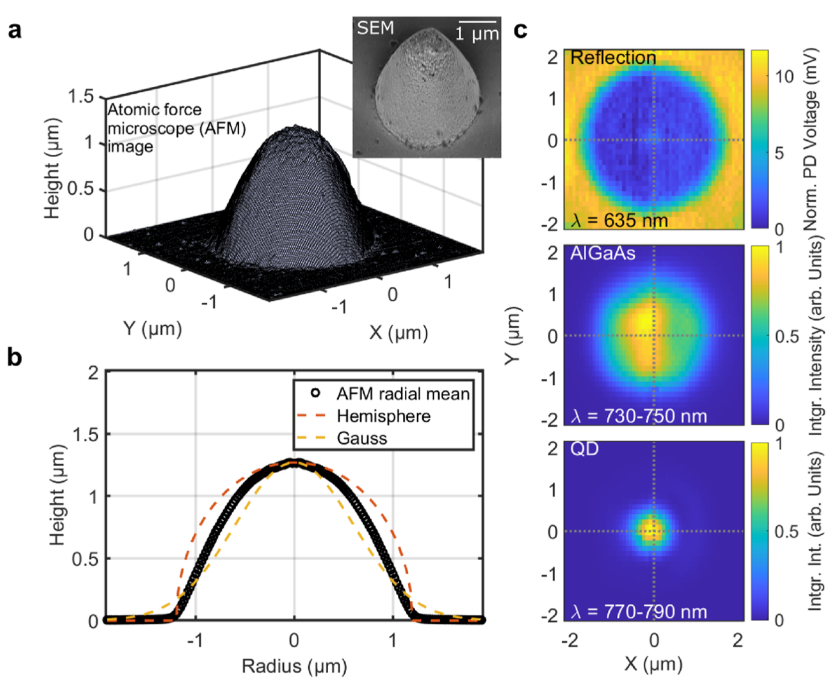

FIG. 3. (a) Exemplary height profile of a single monolithic microlens with embedded quantum dots obtained using an atomic force microscope (AFM). Inset: Scanning electron beam micrograph (SEM) of a single microlens recorded at an angle of 45°. (b) Height profile of the microlens of (a) averaged along the lens azimuth, plotted as a function of its radius. The profiles of comparable hemispheric and Gaussian lens profiles are indicated by dashed lines. (c) High resolution of the hyperspectral imaging micrographs for the different reflection and luminescence bands, cf. Fig. 2. The full width at half maximum (FWHM) spatial resolution of the hyperspectral images collected through the single mode fiber is 604(16) nm, cf. supplementary material, Fig. S5.

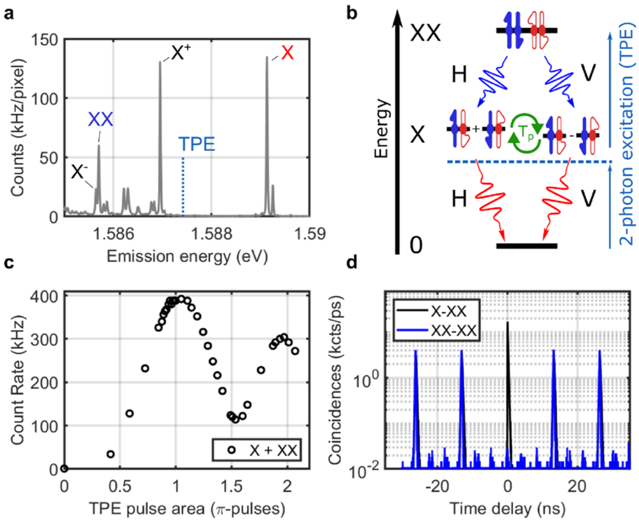

FIG. 4. (a) Above-band excitation spectrum of a single GaAs quantum dot as recorded through the 3D-printed single mode fiber objective. The different emission lines of the excitonic complexes of the exciton X, biexciton XX, and trions X^- and X^+ as well as the energy of the resonant two-photon excitation (TPE) are annotated (cf. Ref. 33). (b) Schematic illustration of the energetic level diagram of X and XX excitonic complexes used to obtain entangled photon pairs by the two-photon pulsed resonant excitation scheme. The X emission process precession is modulated by the precession period T_p (cf. Refs. 13 and 43). (c) Combined detector count rate of all four single photon detectors (cf. supplementary material, Sec. I D) as a function of the TPE pulse area. The first Rabi-π-pulse is achieved at a power of 0.65 μW at a laser repetition rate of 76 MHz. (d) Measured coincidences vs photon arrival time delay in cross- and auto-correlation configuration of X and XX, respectively, for polarization basis combination H–H.

where the principal Rabi-π-pulse energy is found to be 8.5×10^{-15} J at a 76 MHz TPE rate. The observed combined X and XX single photon rate using superconducting single photon detectors is 392(20) kHz. This equates to a raw overall system per-pulse efficiency of $5.2(3) \times 10^{-3}$ (see the supplementary material, Sec. 1 D, for further discussion. The single photon characteristics of TPE are investigated using polarization resolved X and XX auto- and cross-correlation experiments. This is shown exemplarily for the H–H[42] polarization basis combination of emitted X and XX photons, respectively, in Fig. 4(d). In this graph, a clear bunching effect ($g^{(2)}_{\mathrm{X-XX}}(0) \simeq 2.3$) for the X–XX cross-correlation and a strong anti-bunching in the XX–XX auto-correlation ($g^{(2)}_{\mathrm{XX-XX}}(0) = 8.0(6) \times 10^{-4}$) for time delays $\tau \to 0$ are observed.

In the cascaded decay of the excited XX state, two photons, one at the X and XX transition energies, are emitted. Due to the preservation of the combined angular momentum of QD-confined carriers and emitted photons in the two consequent spontaneous decay processes from the initial XX state to the ground state $j_{|XX\rangle} = j_{|0\rangle} = 0$, the two emitted photons $j_v = \pm 1$ are polarization entangled. The X state exhibits precession oscillations due to its finite fine-structure splitting induced by spin–orbit coupling of its integer spin $j_{|X\rangle} = \pm j_{hh} \mp j_e = \pm\frac{3}{2} \mp \frac{1}{2} = \pm 1$. hh stands for heavy hole and e for electron. As a consequence, the entanglement basis precesses around the H–V polarization axis. A detailed description of the creation of polarization entangled photon pairs from GaAs QDs and the precession effect can be found in the supplementary material, Sec. I F, as well as Refs. 13 and 43. The fine-structure splitting Δ_{FSS} of this particular QD is determined to be 5.79(20) μeV, inducing an X state precession period T_p^X of 714(24) ps. By measuring the full polarization tomography in all $6 \times 6 = 36$ polarization basis combinations of the time-resolved X–XX coincidences, the two-photon density matrix of the entangled state can be reconstructed. We are following the standard procedure as outlined, for example, in Ref. 42. The full tomography measurement, including an overlay of the data with a maximally entangled state model, is shown explicitly in the supplementary material, Fig. S8. Due to the excellent agreement between the maximally entangled state model and the presented data, we conclude that the entangled state prepared by the presented entangled photon pair source is a good approximation of being maximally entangled. The model parameters T_p^X and $T_1^X = 320(1)$ ps are determined in separate measurements (see the supplementary material, Secs. III and IV). By comparing the theory and ideal state curve while considering the detector time resolution, it can be concluded that the observable entanglement is mainly limited by the detector time resolution relative to T_p^X and the precision of the polarization projection units, cf. supplementary material, Fig. S2, but not by the quality of the entangled source itself. Static linear polarization rotations of optical elements such as the microlens or the lensed fiber are compensated for in the polarization projection from the QD to the lab eigenbases.[13,44] No nonlinear polarization rotations from optical elements are expected due to the low employed average optical power densities $<\mu W$. The extracted two-photon density matrices ρ and the source entanglement negatives $2n$ are summarized in Fig. 5. The observed maximal entanglement negativity $2n$ over a 4 ps window is 0.96(2), while the average over the photon pairs collected within one exciton lifetime T_1^X equates to 0.81(1). The extracted negatives as a function of time delay δ_τ are depicted in Fig. 5(b). The theoretical curve represents a maximally entangled state; see discussion in the supplementary material, Sec. I F, while the model is the same as the theory curve but convoluted with the detector time resolution. It is worth noting that the maximally entangled model is not fitted to the data, as it has no free parameters except the scaling to the coincidences. It is apparent that the entanglement of the emitted photon pairs levels off after an initial decrease from its maximum at about $2n = 0.7$, which remains intact for time delays of multiple T_1^X and is only limited by the signal-to-noise ratio at $\delta\tau/T_1^X \gg 1$. While the maximally entangled model generally describes the observations quite well, the entanglement decay, mainly caused by time uncertainty in the measurement, exhibits some deviation. We attribute this to the uncertainties in the two-photon detection timing resolution $\delta^{\mathrm{det}}_{\mathrm{FWHM}} = 126(15)$ ps and exciton precession period T_p^X (cf. supplementary material, Secs. I D and I F, for details). Potentially, also effects that are not considered in the model and theory, such as spin relaxation during the $XX - X$-cascade, could play a contributing role in explaining the observed deviation. Nevertheless, the observations clearly demonstrate that the on-demand entangled photon pair sources based on GaAs QDs embedded in monolithic microlenses and coupled to 3D-printed micro-objectives on single mode fibers exhibit strong characteristics of maximally entangled photon pair sources even in the presence of fine-structure splitting.

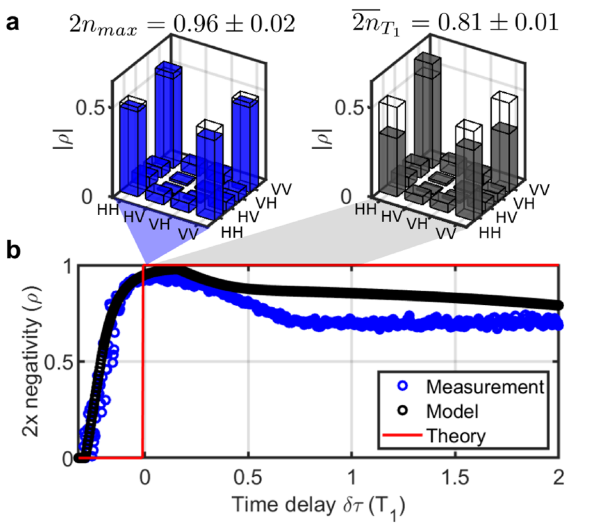

FIG. 5. (a) Representation of the absolute value of extracted two-photon X–XX density matrices ρ using maximum likelihood estimation from the two-photon polarization tomography measurement (see also the supplementary material, Fig. S8). Left: X–XX density matrix for maximal negativity value at time delay δ_τ of 0 using a bin width of 4 ps. Right: Average X–XX density matrix for emitted photons within one exciton lifetime T_1^X = 320(1) ps (cf. supplementary material, Fig. S6). The respective entanglement negativity values 2n of both matrices are denoted above the charts. (b) Entanglement negativity 2n as a function of time delay δ_τ as extracted from the two-photon tomography measurement (blue), maximally entangled state model with detector timing resolution (black), and maximally entangled state theory (red) (cf. supplementary material, Sec. I F).

IV. CONCLUSIONS

We demonstrate and verify a sophisticated and ultra-compact design of fiber-coupled semiconductor QD-based entangled photon pair sources suitable for industrial applications. To achieve this, the emission from the $Al_{0.15}Ga_{0.85}As$ monolithic microlenses with embedded GaAs QDs is collected into single mode fibers at cryogenic temperatures of about 3.8 K. This *in situ* collection is realized using micro-objectives 3D-printed directly on-top of a standard single mode fiber in combination with the QD-microlenses, thereby demonstrating a viable approach to attain the desired compact high-performance entangled photon pair sources. Since the fiber micro-objective and QD microlenses can be positioned against each other using a combination of piezo steppers and scanners, the system retains a great deal of flexibility and is able to compensate for changes. This adjustability can also be employed for high resolution imaging, which is enabled by the diffraction-limited spatial FWHM resolution performance of 604(16) nm of the employed fiber micro-objective. Furthermore, this experimental system enables diffraction-limited hyperspectral imaging by utilizing the simultaneous reflection and luminescence signals of planar samples at cryogenic temperatures. By using the secondary capability to image the sample surface through a traditional microscopy setup co-aligned to the lensed fiber, the capability to efficiently find specific microstructures on an mm-sized sample is preserved. In combination with the fabricated microlenses with centrally embedded QDs, single photon rates of up to 392(20) kHz at 76 MHz pulsed resonant excitation are attained. This constitutes about an order of magnitude improvement compared to investigations of similar systems.[26,28] In addition, using resonant two-photon excitation, this system can be employed to create entangled photon pairs featuring state-of-the-art entanglement negativities 2n of up to 0.96(2) and 0.81(1) when time intervals of 4 ps and X-lifetime [T_1^X = 320(1) ps], respectively, are considered. The investigated QD quantum light source exhibits an uncorrected single photon purity of 99.2(5)%. The observed two-photon density matrices are in good agreement with the model of maximally entangled states, once the experimental limitations of the single photon timing jitter and the accuracy of the polarization projection are accounted for. In a next step, the presented ultra-compact sources will be integrated into mobile, standard 19 *in* rack-systems in order to pioneer quantum networks in industrial environments.

SUPPLEMENTARY MATERIAL

In the supplementary material, details regarding the employed experimental methods, instruments, and setups are provided. In addition, it also contains an in-depth mathematical description and modeling of the photon correlation experiments. For definitions of the six polarization bases H, V, D, A, R, and L, see the supplementary material, Sec. I F.

ACKNOWLEDGMENTS

We acknowledge the clean room team, especially Martin Bauer and Ronny Engelhard, of the Leibniz IFW Dresden for their efforts and expertise in clean room processing of samples. The support of the Attocube Systems AG in the modification of the cryogenic system is gracefully acknowledged. This work was funded by the German Federal Ministry of Education and Research (BMBF) projects QR.X (Contract Nos. 16KISQ013 and 16KISQ016), QD-CamNetz (Contract No. 16KISQ078), QUARKS (Contract No. 16KIS1998K), 3DprintedOptics (Contract No. 13N14097), and Integrated3Dprint (Contract No. 13N16875). H.G., P.R., and S.J. also acknowledge support from Baden-Württemberg Stiftung (project Opterial), the European Research Council (Advanced grant Complexplas and PoC grant 3DPrintedOptics), the German Research Foundation (DFG, Grant No. 431314977/GRK2642), HORIZON EUROPE European Innovation Council (IV-Lab project with Grant No. 101115545), the Carl-Zeiss Foundation (projects EndoPrint3D and QPhoton), and the University of Stuttgart (Terra Incognita program).

AUTHOR DECLARATIONS

Conflict of Interest

The authors have no conflicts to disclose.

Author Contributions

M. Langer: Data curation (equal); Formal analysis (equal); Investigation (equal); Methodology (equal); Resources (equal); Software (equal); Validation (equal); Visualization (lead); Writing – review &

editing (equal). **P. Ruchka**: Conceptualization (equal); Investigation (supporting); Methodology (equal); Writing – review & editing (supporting). **A. Rahimi**: Data curation (equal); Formal analysis (supporting); Methodology (supporting); Software (supporting); Writing – review & editing (supporting). **S. Jakovljevic**: Conceptualization (supporting); Investigation (equal); Methodology (supporting). **Y. G. Zena**: Conceptualization (supporting); Investigation (supporting); Methodology (equal); Resources (equal). **S. A. Dhurjati**: Investigation (supporting); Resources (equal). **A. Danilov**: Data curation (equal); Investigation (supporting); Methodology (supporting); Resources (supporting). **M. Pal**: Conceptualization (supporting); Data curation (supporting); Formal analysis (supporting); Methodology (supporting); Project administration (supporting). **R. Bassoli**: Project administration (supporting); Supervision (supporting). **F. H. P. Fitzek**: Project administration (supporting); Resources (supporting); Supervision (supporting). **O. G. Schmidt**: Supervision (equal). **H. Giessen**: Conceptualization (equal); Formal analysis (supporting); Funding acquisition (equal); Project administration (equal); Resources (equal); Supervision (equal); Validation (supporting); Writing – review & editing (equal). **C. Hopfmann**: Conceptualization (equal); Funding acquisition (equal); Investigation (equal); Methodology (equal); Project administration (lead); Software (lead); Supervision (lead); Validation (equal); Writing – original draft (lead); Writing – review & editing (lead).

DATA AVAILABILITY

The data that support the findings of this study are available from the corresponding author upon reasonable request.

REFERENCES

[1] D. Kim, S. Economou, Ş. Bădescu, M. Scheibner, A. Bracker, M. Bashkansky, T. Reinecke, and D. Gammon, "Optical spin initialization and nondestructive measurement in a quantum dot molecule," Phys. Rev. Lett. **101**, 236804 (2008).

[2] S.-H. Wei, B. Jing, X.-Y. Zhang, J.-Y. Liao, C.-Z. Yuan, B.-Y. Fan, C. Lyu, D.-L. Zhou, Y. Wang, G.-W. Deng, H.-Z. Song, D. Oblak, G.-C. Guo, and Q. Zhou, "Towards real-world quantum networks: A review," Laser Photonics Rev. **16**, 2100219 (2022).

[3] J. Claudon, J. Bleuse, N. S. Malik, M. Bazin, P. Jaffrennou, N. Gregersen, C. Sauvan, P. Lalanne, and J.-M. Gérard, "A highly efficient single-photon source based on a quantum dot in a photonic nanowire," Nat. Photonics **4**, 174–177 (2010).

[4] A. Dousse, J. Suffczyński, A. Beveratos, O. Krebs, A. Lemaître, I. Sagnes, J. Bloch, P. Voisin, and P. Senellart, "Ultrabright source of entangled photon pairs," Nature **466**, 217–220 (2010).

[5] N. Somaschi, V. Giesz, L. De Santis, J. C. Loredo, M. P. Almeida, G. Hornecker, S. L. Portalupi, T. Grange, C. Antón, J. Demory, C. Gómez, I. Sagnes, N. D. Lanzillotti-Kimura, A. Lemaítre, A. Auffeves, A. G. White, L. Lanco, and P. Senellart, "Near-optimal single-photon sources in the solid state," Nat. Photonics **10**, 340–345 (2016).

[6] Y. Chen, M. Zopf, R. Keil, F. Ding, and O. G. Schmidt, "Highly-efficient extraction of entangled photons from quantum dots using a broadband optical antenna," Nat. Commun. **9**, 2994 (2018).

[7] H. Wang, H. Hu, T.-H. Chung, J. Qin, X. Yang, J.-P. Li, R.-Z. Liu, H.-S. Zhong, Y.-M. He, X. Ding, Y.-H. Deng, Q. Dai, Y.-H. Huo, S. Höfling, C.-Y. Lu, and J.-W. Pan, "On-demand semiconductor source of entangled photons which simultaneously has high fidelity, efficiency, and indistinguishability," Phys. Rev. Lett. **122**, 113602 (2019).

[8] J. Liu, R. Su, Y. Wei, B. Yao, S. F. C. d. Silva, Y. Yu, J. Iles-Smith, K. Srinivasan, A. Rastelli, J. Li, and X. Wang, "A solid-state source of strongly entangled photon pairs with high brightness and indistinguishability," Nat. Nanotechnol. **14**, 586–593 (2019).

[9] C.-Y. Lu and J.-W. Pan, "Quantum-dot single-photon sources for the quantum internet," Nat. Nanotechnol. **16**, 1294–1296 (2021).

[10] N. Tomm, A. Javadi, N. O. Antoniadis, D. Najer, M. C. Löbl, A. R. Korsch, R. Schott, S. R. Valentin, A. D. Wieck, A. Ludwig, and R. J. Warburton, "A bright and fast source of coherent single photons," Nat. Nanotechnol. **16**, 399–403 (2021).

[11] G. Shooter, Z.-H. Xiang, J. R. A. Müller, J. Skiba-Szymanska, J. Huwer, J. Griffiths, T. Mitchell, M. Anderson, T. Müller, A. B. Krysa, R. Mark Stevenson, J. Heffernan, D. A. Ritchie, and A. J. Shields, "1 GHz clocked distribution of electrically generated entangled photon pairs," Opt. Express **28**, 36838–36848 (2020).

[12] R. Uppu, F. T. Pedersen, Y. Wang, C. T. Olesen, C. Papon, X. Zhou, L. Midolo, S. Scholz, A. D. Wieck, A. Ludwig, and P. Lodahl, "Scalable integrated single-photon source," Sci. Adv. **6**, eabc8268 (2020).

[13] C. Hopfmann, W. Nie, N. L. Sharma, C. Weigelt, F. Ding, and O. G. Schmidt, "Maximally entangled and gigahertz-clocked on-demand photon pair source," Phys. Rev. B **103**, 075413 (2021).

[14] P. van Loock, W. Alt, C. Becher, O. Benson, H. Boche, C. Deppe, J. Eschner, S. Höfling, D. Meschede, P. Michler, F. Schmidt, and H. Weinfurter, "Extending quantum links: Modules for fiber- and memory-based quantum repeaters," Adv. Quantum Technol. **3**, 1900141 (2020).

[15] C. Schimpf, M. Reindl, F. Basso Basset, K. D. Jöns, R. Trotta, and A. Rastelli, "Quantum dots as potential sources of strongly entangled photons: Perspectives and challenges for applications in quantum networks," Appl. Phys. Lett. **118**, 100502 (2021).

[16] X.-L. Wang, L.-K. Chen, W. Li, H.-L. Huang, C. Liu, C. Chen, Y.-H. Luo, Z.-E. Su, D. Wu, Z.-D. Li, H. Lu, Y. Hu, X. Jiang, C.-Z. Peng, L. Li, N.-L. Liu, Y.-A. Chen, C.-Y. Lu, and J.-W. Pan, "Experimental ten-photon entanglement," Phys. Rev. Lett. **117**, 210502 (2016).

[17] W. McCutcheon, A. Pappa, B. A. Bell, A. McMillan, A. Chailloux, T. Lawson, M. Mafu, D. Markham, E. Diamanti, I. Kerenidis, J. G. Rarity, and M. S. Tame, "Experimental verification of multipartite entanglement in quantum networks," Nat. Commun. **7**, 13251 (2016).

[18] C. Zhang, Y.-F. Huang, B.-H. Liu, C.-F. Li, and G.-C. Guo, "Spontaneous parametric down-conversion sources for Multiphoton experiments," Adv. Quantum Technol. **4**, 2000132 (2021).

[19] A. S. Cacciapuoti, M. Caleffi, F. Tafuri, F. S. Cataliotti, S. Gherardini, and G. Bianchi, "Quantum internet: Networking challenges in distributed quantum computing," IEEE Network **34**, 137–143 (2020).

[20] F. Basso Basset, M. Valeri, E. Roccia, V. Muredda, D. Poderini, J. Neuwirth, N. Spagnolo, M. B. Rota, G. Carvacho, F. Sciarrino, and R. Trotta, "Quantum key distribution with entangled photons generated on demand by a quantum dot," Sci. Adv. **7**, eabe6379 (2021).

[21] M. J. Stevens, "Chapter 2—Photon statistics, measurements, and measurements tools," in *Single-Photon Generation and Detection, Experimental Methods in the Physical Sciences*, edited by A. Migdall, S. V. Polyakov, J. Fan, and J. C. Bienfang (Academic Press, 2013), Vol. 45, pp. 25–68.

[22] N. Akopian, N. H. Lindner, E. Poem, Y. Berlatzky, J. Avron, D. Gershoni, B. D. Gerardot, and P. M. Petroff, "Entangled photon pairs from semiconductor quantum dots," Phys. Rev. Lett. **96**, 130501 (2006).

[23] R. M. Stevenson, R. J. Young, P. Atkinson, K. Cooper, D. A. Ritchie, and A. J. Shields, "A semiconductor source of triggered entangled photon pairs," Nature **439**, 179 (2006).

[24] S. Bounouar, M. Müller, A. M. Barth, M. Glässl, V. M. Axt, and P. Michler, "Phonon-assisted robust and deterministic two-photon biexciton preparation in a quantum dot," Phys. Rev. B **91**, 161302 (2015).

[25] D. Huber, M. Reindl, Y. Huo, H. Huang, J. S. Wildmann, O. G. Schmidt, A. Rastelli, and R. Trotta, "Highly indistinguishable and strongly entangled photons from symmetric GaAs quantum dots," Nat. Commun. **8**, 15506 (2017).

[26] A. Schlehahn, S. Fischbach, R. Schmidt, A. Kaganskiy, A. Strittmatter, S. Rodt, T. Heindel, and S. Reitzenstein, "A stand-alone fiber-coupled single-photon source," Sci. Rep. **8**, 1340 (2018).

[27] A. Musiał, K. Żołnacz, N. Srocka, O. Kravets, J. Große, J. Olszewski, K. Poturaj, G. Wójcik, P. Mergo, K. Dybka, M. Dyrkacz, M. Dłubek, K. Lauritsen, A. Bülter, P.-I. Schneider, L. Zschiedrich, S. Burger, S. Rodt, W. Urbańczyk, G. Sęk, and S. Reitzenstein, "Plug&Play fiber-coupled 73 kHz single-photon source operating in the telecom O-band," Adv. Quantum Technol. **3**, 2000018 (2020).

[28] L. Bremer, K. Weber, S. Fischbach, S. Thiele, M. Schmidt, A. Kaganskiy, S. Rodt, A. Herkommer, M. Sartison, S. L. Portalupi, P. Michler, H. Giessen, and S. Reitzenstein, "Quantum dot single-photon emission coupled into single-mode fibers with 3D printed micro-objectives," APL Photonics **5**, 106101 (2020).

[29] D. E. Aspnes, S. M. Kelso, R. A. Logan, and R. Bhat, "Optical properties of $Al_xGa_{1-x}As$," J. Appl. Phys. **60**, 754–767 (1986).

[30] A. J. Shields, "Semiconductor quantum light sources," Nat. Photonics **1**, 215–223 (2007).

[31] W. Nie, N. L. Sharma, C. Weigelt, R. Keil, J. Yang, F. Ding, C. Hopfmann, and O. G. Schmidt, "Experimental optimization of the fiber coupling efficiency of GaAs quantum dot-based photon sources," Appl. Phys. Lett. **119**, 244003 (2021).

[32] S. Stufler, P. Machnikowski, P. Ester, M. Bichler, V. M. Axt, T. Kuhn, and A. Zrenner, "Two-photon Rabi oscillations in a single In_xGa_xAs–GaAs quantum dot," Phys. Rev. B **73**, 125304 (2006).

[33] C. Hopfmann, N. L. Sharma, W. Nie, R. Keil, F. Ding, and O. G. Schmidt, "Heralded preparation of spin qubits in droplet-etched GaAs quantum dots using quasiresonant excitation," Phys. Rev. B **104**, 075301 (2021).

[34] M. Langer, S. A. Dhurjati, Y. G. Zena, A. Rahimi, M. Pal, L. Raith, S. Nestler, R. Bassoli, F. H. P. Fitzek, O. G. Schmidt, and C. Hopfmann, "Bright quantum dot light sources using monolithic microlenses on gold back-reflectors," Nanotechnology **36**, 225301 (2025).

[35] T. Gissibl, S. Thiele, A. Herkommer, and H. Giessen, "Sub-micrometre accurate free-form optics by three-dimensional printing on single-mode fibres," Nat. Commun. **7**, 11763 (2016).

[36] M. Sartison, K. Weber, S. Thiele, L. Bremer, S. Fischbach, T. Herzog, S. Kolatschek, M. Jetter, S. Reitzenstein, A. Herkommer, P. Michler, S. L. Portalupi, and H. Giessen, "3D printed micro-optics for quantum technology: Optimised coupling of single quantum dot emission into a single-mode fibre," Light: Adv. Manuf. **2**, 6 (2021).

[37] K. Weber, S. Thiele, M. Hentschel, A. Herkommer, and H. Giessen, "Positional accuracy of 3D printed quantum emitter fiber couplers," Adv. Quantum Technol. **7**, 2400135 (2024).

[38] J. Schwab, K. Weber, J. Drozella, C. Jimenez, A. Herkommer, L. Bremer, S. Reitzenstein, and H. Giessen, "Coupling light emission of single-photon sources into single-mode fibers: Mode matching, coupling efficiencies, and thermo-optical effects," Opt. Express **30**, 32292–32305 (2022).

[39] A. Asadollahbaik, S. Thiele, K. Weber, A. Kumar, J. Drozella, F. Sterl, A. M. Herkommer, H. Giessen, and J. Fick, "Highly efficient dual-fiber optical trapping with 3D printed diffractive fresnel lenses," ACS Photonics **7**, 88–97 (2020).

[40] P. Ruchka, S. Hammer, M. Rockenhäuser, R. Albrecht, J. Drozella, S. Thiele, H. Giessen, and T. Langen, "Microscopic 3D printed optical tweezers for atomic quantum technology," Quantum Sci. Technol. **7**, 045011 (2022).

[41] Fiber diameter 250 μm with polyamide coating and 125 μm bare.

[42] D. F. V. James, P. G. Kwiat, W. J. Munro, and A. G. White, "Measurement of qubits," Phys. Rev. A **64**, 052312 (2001).

[43] R. Winik, D. Cogan, Y. Don, I. Schwartz, L. Gantz, E. R. Schmidgall, N. Livneh, R. Rapaport, E. Buks, and D. Gershoni, "On-demand source of maximally entangled photon pairs using the biexciton-exciton radiative cascade," Phys. Rev. B **95**, 235435 (2017).

[44] D. Cogan, G. Peniakov, Z.-E. Su, and D. Gershoni, "Complete state tomography of a quantum dot spin qubit," Phys. Rev. B **101**, 035424 (2020).